JOURNAL OF APPLIED ELECTROCHEMISTRY **10** (1980) 81–90

High oxygen ion conduction in sintered oxides of the Bi_2O_3-Er_2O_3 system

M. J. VERKERK, K. KEIZER, A. J. BURGGRAAF

Twente University of Technology, Department of Inorganic Materials Science, PO Box 217, 7500 AE Enschede, The Netherlands

Received 22 February 1979

The phase diagram of the Bi_2O_3–Er_2O_3 system was investigated. A monophasic f c c structure was stabilized for samples containing 17.5–45.5 mol% Er_2O_3. Above and below this concentration range polyphasic regions appear. The fcc phase showed high oxygen ion conduction. The ionic transference number is equal to one for specimens containing 30 mol% Er_2O_3 or less, while an electronic component is introduced at low temperatures for specimens containing 40–60 mol% Er_2O_3. Between 673 K and 873 K a maximum in the conductivity was found at 20 mol% Er_2O_3. $(Bi_2O_3)_{0.80}(Er_2O_3)_{0.20}$ is found to be the best oxygen ion conductor so far known. The conductivity at 773 K and 973 K is 2.3 $\Omega^{-1}m^{-1}$ and 37 $\Omega^{-1}m^{-1}$ respectively. These values are 2–3 times higher than the best oxygen ion conductor reported for substituted Bi_2O_3 systems and 50–100 times higher than those of stabilized zirconia $(ZrO_2)_{0.915}(Y_2O_3)_{0.085}$ at corresponding temperatures.

1. Introduction

In the search for new inorganic compounds which exhibit predominantly oxygen ion conduction within a broad temperature range at lower temperatures, Bi_2O_3 was found to be a promising material. In the δ-phase (face centred cubic, or fcc), which exists between the transition point at about 1003 K up to the melting point at 1097 K [1–5], the electrical conductivity is about 100 $\Omega^{-1}m^{-1}$ [4, 6]. In the cooling direction this highly conductive phase may be extended down to about 918 K [2–8]. The conductivity in the α-phase (monoclinic [2, 4, 9–11]) which exists from ambient temperature up to the transition point is at least three decades lower [4, 6]. The ionic transport number was found to be equal to one in the δ-phase [6]; in the α-phase an ionic contribution to the conductivity could be detected only near the α→δ transition [4].

The temperature range at which the materials can be used as a solid electrolyte can be extended by substituting Bi_2O_3. Takahashi *et al.* investigated the electrical properties of Bi_2O_3 with several substituents [6, 12–19]. The region of highly ionic conductive δ-phase (fcc) can be extended to room temperature with a composition of 25–43 mol% Y_2O_3 [13], 35–50 mol% Gd_2O_3 [16], 25 mol% WO_3 [12], 15–25 mol% Nb_2O_5 and 18–25 mol% Ta_2O_5 [19]. The conductivity of these solid solutions is lower than that in the δ-phase of pure Bi_2O_3. However, the region of the highly ionic conductive phase is extended to room temperature and the sudden volume change at the phase transition is avoided, which is important for practical applications. The conductivity of stabilized bismuth sesquioxides is one decade or more higher than that of stabilized zirconias at the same temperature. However, at higher temperatures these stabilized bismuth sesquioxides show a tendency to be reduced under low oxygen pressures [6, 14]. At the moment practical applications can be realized in the form of oxygen gauges and oxygen pumps [20].

From the correlation we found between the ionic radii of the substituents and the amount of substituted M(III) ions necessary to stabilize the δ-phase at room temperature we can conclude that Bi_2O_3 substituted with Er_2O_3 should be a promising system.

The occurence of the δ-phase at room temperature in the system under consideration for higher

0021–891X/80/010081–10$03.00/0

Er_2O_3 concentrations was reported for $3Bi_2O_3 \cdot Er_2O_3$ by Datta and Meehan [22] and was suggested for $Bi_2O_3 \cdot Er_2O_3$ by Nasonova *et al.* [23]. No other results concerning the phase diagram are reported in the literature. From these points of view the authors have investigated the oxygen ion conduction in sintered oxides of the Bi_2O_3–Er_2O_3 system.

The specific purpose of these investigations in the Bi_2O_3–Er_2O_3 system is to find a high oxygen ion conductor as electrolyte for 'second generation' oxygen sensors for automotive control (e.g. the device developed by Heyne [21]).

2. Experimental

2.1. *Preparation and analysis of the specimens*

Bi_2O_3 (Merck, very pure) and Er_2O_3 (Serva, 99.9%) were thoroughly mixed and pre-fired at 1020–1120 K for 16 h, finely ground and isostatically pressed at about 400 MPa, sintered in air for 65 h and cooled down to room temperature at 0.5 K min^{-1}. As shown in Table 1, the sintering temperature required to reach densities of $\geq$ 94% increased as the content of Er_2O_3 was increased. After the synthesis the composition of the samples was checked using X-ray fluorescence; the accuracy of this determination is 0.1%.

The starting materials and two specimens were analysed spectroscopically for small amounts of aluminium and silicon. The amount of aluminium and silicon is important because of their influence on the electrical conductivity, especially in connection with grain boundary effects.

Si was analysed according to the method developed in our laboratory [24]. For the analysis of aluminium a new method was developed (see Appendix). The detection limits of these analyses are 0.005 wt% Al and 0.001 wt% Si.

Table 1. Sintering temperature and density of the specimens

Composition x† *in* $(Bi_2O_3)_{1-x}(Er_2O_3)_x$	*Temperature* (K)	*Density*‡
0.025 ~ 0.125	1063	
0.15 ~ 0.175	1123	96%
0.20 ~ 0.25	1198	96%
0.30 ~ 0.35	1273	94%
0.40 ~ 0.455	1323	94%
0.50 ~ 0.60	1373	

† $x \times 100 =$ mol%

‡ Density is given as a percentage of the theoretical density based on defect fluorite-type lattice

The crystal structures of the specimens were identified with a Philips PW 1370 diffractometer. CuKα radiation was used with a Ni filter. The lattice parameters were calculated from diffraction angles in the 60–120° (2θ) region, obtained at a scanning speed of 0.25° min^{-1} using $Pb(NO_3)_2$ as the internal standard.

High temperature X-ray experiments were performed with a Guinier–Lenné camera (heating rate: 5 K h^{-1}). The Pt gauze of the sample holder served as a standard, since internal standards could not be used due to the corrosive nature of Bi_2O_3.

Differential thermal analysis measurements were performed with a Dupont 990 Thermal Analyzer (heating rate: 10 or 15 K min^{-1}). A Dupont 951 Thermogravimetric Analyzer was used for investigating various features of defect chemistry. The expansion as a function of temperature was measured with a Leitz dilatometer UBD (heating rate: 1 K min^{-1}) on sintered rods having a diameter of 4 mm and a length of 10 mm. The densities of the samples were measured at 298 K by the standard Archimedes method using mercury.

2.2. *Measurement of the ionic conduction*

The ionic conductivity was examined by measuring the electrical conductivity and the e.m.f. of an oxygen concentration cell. Porous platinum electrodes were sputtered onto the specimens.

The electrical conductivity was measured on cylindrical rods (3 mm x 4 mm) with a Wayne–Kerr Universal Bridge B221 using the two-probe method. A frequency of 10 kHz was used because the conductivity was nearly frequency independent in the range of 1 kHz–1 MHz. This means that in this case grain size effects play a minor role. This can be expected if the grain size is larger than 20 μm and the impurity concentration is relatively low.

The ionic transference number was examined by measuring the e.m.f. of an oxygen gas concentration cell:

$$O_2(P_{O_2,a}), \text{Pt} \mid \text{specimen disc (10 mm x 2 mm)} \mid \text{Pt}, O_2(P_{O_2,b}) \quad (1)$$

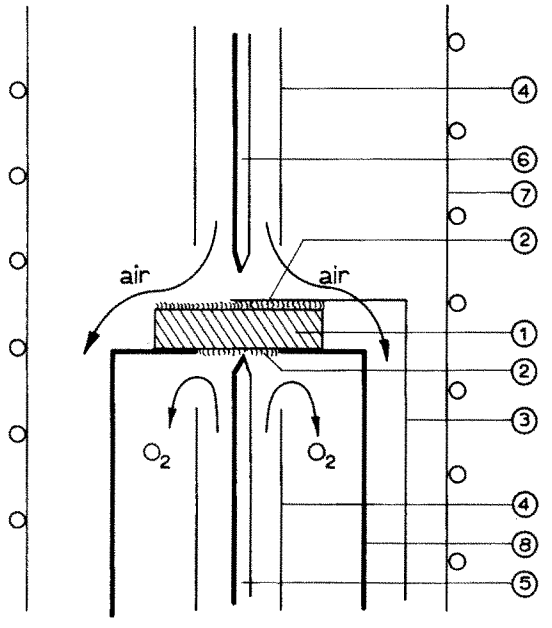

Fig. 1. Construction of the concentration cell.
1 specimen; 2 porous Pt-electrode; 3 Pt-lead; 4,8 quartz tube; 5,6 Pt/Pt, 10% Rh thermocouple; 7 furnace wall.

where $P_{O_2,a} = 0.21$ atm (air) and $P_{O_2,b} = 1.00$ atm (pure oxygen).

If the conduction is purely ionic the e.m.f. E_0 of this cell is given by

$$E_0 = \frac{RT}{4F} \ln(P_{O_2,b})/(P_{O_2,a}). \qquad (2)$$

In a mixed conductor the e.m.f. is lowered due to the electronic conduction and the average ion transference number is given by:

$$t_i = \frac{\sigma_i}{\sigma_i + \sigma_e} = \frac{E}{E_0} \qquad (3)$$

where σ_i is the ionic conduction, σ_e the electronic conduction and E is the measured e.m.f.

Fig. 1 shows the construction of the concentration cell (a vertical apparatus), a detailed figure will be given by T. v. Dijk *et al.* [25].

3. Results and discussion

3.1. *Samples prepared*

As shown in Table 1 the densities of the specimens after sintering were 94–96% of the theoretical density. The average grain size of all the samples was about 30 μm. The difference between the calculated composition and the measured composition (X-ray fluorescence) of the specimens was 0.2% or less. The colour of the specimens changed from orange for 2.5 mol% Er_2O_3 through yellow for 15 mol% Er_2O_3 to brown for the specimens with 30–60 mol% Er_2O_3. Quenched specimens were orange in most cases.

Table 2. Concentration of the aluminium and silicon impurities in the starting materials and specimens

Sample	*wt% Si*	*wt% Al*
Bi_2O_3	≤0.001	0.03
Er_2O_3	0.003	0.02
$(Bi_2O_3)_{0.80}(Er_2O_3)_{0.20}$	0.008	0.03
$(Bi_2O_3)_{0.545}(Er_2O_3)_{0.455}$	0.010	0.02

Table 2 gives the concentration of the aluminium and silicon impurities of the analysed samples. It is easy to see that the aluminium impurities in the specimens are found in the starting materials whereas the silicon impurities are mainly introduced during the synthesis; possibly the grinding procedure.

The strength of the ceramic samples containing 15–25 mol% Er_2O_3 is relatively low, possibly due to strain.

3.2. *Structural aspects*

Table 3 gives a survey of the existing structure(s) if the specimens are subjected to different heat treatments. In the 'quenching' procedure the samples were suddenly removed from the furnace and cooled to room temperature by natural convection with the result that the high temperature structure may be retained. This can be avoided by cooling down the specimens very slowly (0.5 K min^{-1}). In order to ensure that the high temperature structures are retained during cooling down by 0.5 K min^{-1} the specimens were annealed for 250 h at 898 K.

The monophasic fcc structure was observed at low temperatures for samples containing 17.5–45.5 mol% Er_2O_3. As shown in Fig. 2 the lattice constants of the specimens decrease with an increase in the content of Er_2O_3. Vegard's rule holds in this composition range, which means that over this range an fcc solid solution is found. Below 17.5 mol% Er_2O_3 and above 45.5 mol% Er_2O_3

Table 3. Survey of the structural data of the Bi_2O_3–Er_2O_3 system

x in $(Bi_2O_3)_{1-x}(Er_2O_3)_x$	*Temperature treatment*		
	'Quenched' from the sintering temperature	*Cooled down by 0.5 K min^{-1}*	*Annealed for 250 h at 898 K*
0.025	$\alpha + \beta$†‡	β	$\alpha + \beta$
0.05	β	β	$\alpha + \beta$
0.075	β	β^*§	$\alpha + \delta$
0.10	β^*	β^*	$\alpha + \delta$
0.125	δ^*	δ^*	$\alpha + \delta + \epsilon$¶
0.15	δ	δ	$\alpha + \delta + \beta + \epsilon$
0.175 ~ 0.455	δ	δ	δ
0.50 ~ 0.60	$\delta + Er_2O_3$	$\delta + Er_2O_3$	$\delta + Er_2O_3$

† The β-phase has a tetragonal structure [2, 4, 9, 7]
‡ The structures shown in bold appear in minor concentrations
§ An asterisk means that the structure is distorted
¶ In this table ϵ denotes the rhombohedral structure

polyphasic regions appear. Further study is necessary to determine the exact location of the phase boundaries and the temperatures of the phase transition in these regions. In this study these regions are not investigated in detail.

These results agree with the observation of Datta and Meehan [22] who reported the existence of the fcc phase for $3Bi_2O_3 \cdot Er_2O_3$, while the existence of the fcc phase for $Bi_2O_3 \cdot Er_2O_3$ as suggested by Nasonova *et al.* [23] is not confirmed by our study.

As a result of this study we did find that the percentage of Er_2O_3 necessary to stabilize the fcc structure of Bi_2O_3 at low temperatures is the lowest percentage substituent known in literature for valence (III) lanthanides as substituents [6, 13–16]. For valence (V) substituents 15 mol% Nb_2O_5 and 18 mol% Ta_2O_5 is necessary to stabilize the fcc phase [19].

Theoretical densities of these materials have been calculated from the measured lattice constants (see Fig. 2), making use of three possible models:

1. all cations occupy their normal sites in the fluorite structure and there are two vacancies to a unit cell, i.e. $Bi_{4(1-x)}\,Er_{4x}O_6\square_2$.

2. all cations occupy their normal sites in the fluorite structure and the vacancies are occupied by oxygen ions:

$$O_2 + 2\square \rightarrow 2O^{2-} + 4h^+ \qquad (4)$$

where h^+ denotes a hole; i.e. $Bi_{4(1-x)}\,Er_{4x}O_8$

3. all Bi^{3+} ions occupy their normal sites in the fluorite structure and the Er^{3+} ions occupy interstitial sites, i.e. $Bi_4Er_{4x/(1-x)}O_{6/(1-x)}$.

Comparing the calculated densities and the observed densities, as given in Fig. 3, we can see that model 3 is quite improbable. SEM photographs showed that the specimens had only a slight porosity, so model 2 is incorrect. Model 2 appeared to be incorrect because concentration cell measurements showed oxygen ion conduction and no hole conduction (see Section 3.4). Furthermore with a thermobalance a negligible weight increase was detected during the solid state reaction of Bi_2O_3 and Er_2O_3 on heating in air. Consequently model 1 is the most likely.

3.3. *The conductivity of the sintered specimens*

The conductivity of the sintered Bi_2O_3–Er_2O_3

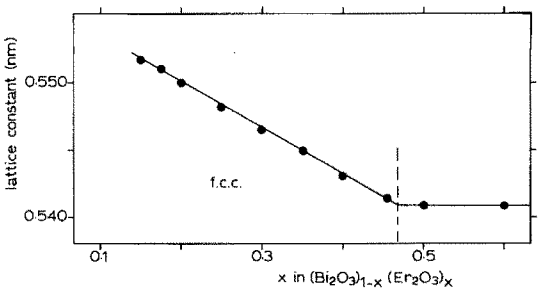

Fig. 2. Lattice constant of the fcc phase of the specimens cooled from the sintering temperature by 0.5 K min^{-1} to room temperature.

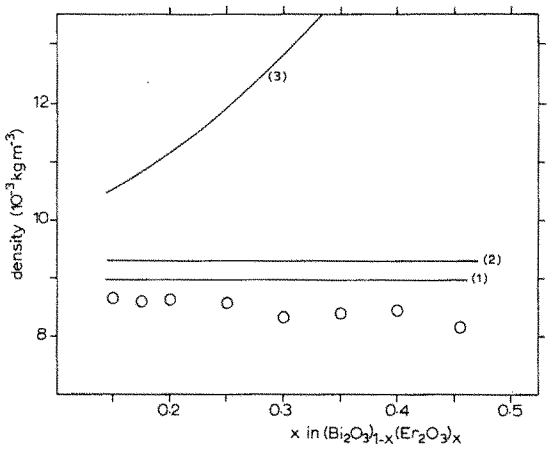

Fig. 3. Observed densities and calculated densities for various crystal models: (1) for model $Bi_{4(1-x)}Er_{4x}O_6\square_2$; (2) for model $Bi_{4(1-x)}Er_{4x}O_8$; (3) for model $Bi_4Er_{4x/(1-x)}O_{6/(1-x)}$. The open circles represent the measured densities.

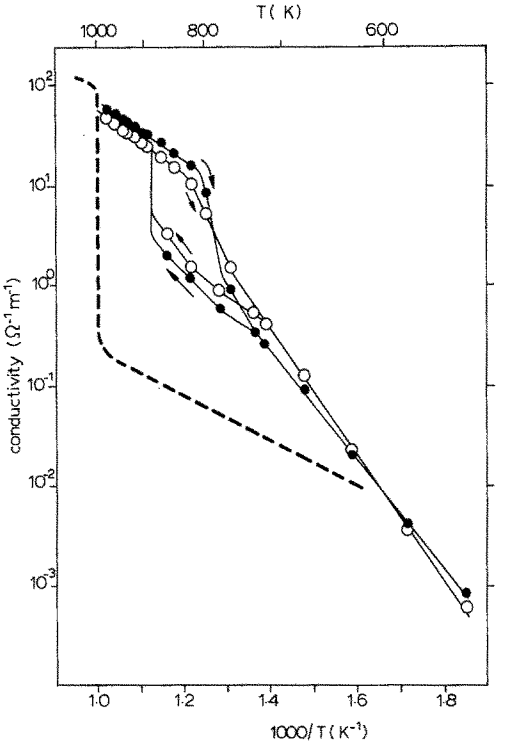

Fig. 4. Conductivity of $(Bi_2O_3)_{1-x}(Er_2O_3)_x$ in air. •, $x = 0.15$; ○, $x = 0.175$. The broken line represents the conductivity of pure Bi_2O_3.

specimens measured in air is shown in Figs. 4 and 5 as Arrhenius plots. In these figures the conductivity of pure Bi_2O_3 (Takahashi *et al.* [6]) is given as a reference material. Table 4 gives the values of the activation energies E_a and the pre-exponential terms σ_0 for the Arrhenius plots of the conductivity, while the deviation is given in the 90% reliability interval.

3.3.1. Conductivity of the samples with 15 and 17.5 mol% Er_2O_3. The specimens containing 15 and 17.5 mol% Er_2O_3 at (738 ± 10) K show a change in the activation energy of the conductivity and at (878 ± 10) K there is a sudden increase in the conductivity (see Fig. 4). In the cooling

Table 4. Activation energies and pre-exponential terms for the Arrhenius plots of the conductivity of the fcc phase

x in $(Bi_2O_3)_{1-x}(Er_2O_3)_x$	*High temperature range* > 873 K		*Low temperature range* < 823 K	
	log σ_0 (Ω^{-1}m^{-1})	E_a (kJ mol^{-1})	*log* σ_0 (Ω^{-1}m^{-1})	E_a (kJ mol^{-1})
0.15	4.8 ± 0.1	56 ± 2	7.0 ± 0.2†	104 ± 3†
0.175	5.4 ± 0.7	68 ± 10	8.1 ± 0.3‡	118 ± 4‡
0.20	4.9 ± 0.2	62 ± 3	8.11 ± 0.04	114.6 ± 0.5
0.25	5.25 ± 0.04	72 ± 4	7.90 ± 0.06	117 ± 1
0.30	6.93 ± 0.09	108 ± 1	6.93 ± 0.09	108 ± 1
0.35	6.7 ± 0.2	109 ± 2	6.7 ± 0.2	109 ± 2
0.40	6.1 ± 0.1	111 ± 2	6.1 ± 0.1	111 ± 2
0.455	6.3 ± 0.2	117 ± 3	6.3 ± 0.2	117 ± 3
0.50	6.3 ± 0.2	120 ± 3	6.3 ± 0.2	120 ± 3
0.60	6.3 ± 0.2	124 ± 3	6.3 ± 0.2	124 ± 3

† Between 748–873 K these values are: log $\sigma_0 = 6.40 \pm 0.04$ Ω^{-1} cm^{-1}, $E_a = 84 \pm 1$ kJ mol^{-1}; the deviation of these values is given in the 65% reliability interval.

‡ Between 748–873 K these values are: log $\sigma_0 = 6 \pm 1$ Ω^{-1} cm^{-1}, $E_a = 87 \pm 10$ kJ mol^{-1}; the deviation of these values is given in the 65% reliability interval.

Table 5. Survey of the results of the investigations performed on specimens containing 15 and 17.5 mol% Er_2O_3

Method	*15 mol% Er_2O_3* (K)	*17.5 mol% Er_2O_3* (K)
Conductivity (↑)		
change in E_a	730 ± 10	730 ± 10
sudden increase in σ	878 ± 10	878 ± 10
Conductivity (↓)		
strong decrease in σ	800 — 740	830 — 770
HT Guinier (↑)		
broadened reflections	750 — 840	750 — 840
$\delta \rightarrow \beta^*$	841 ± 5	843 ± 5
$\beta^* \rightarrow \delta^*$	878 ± 5	883 ± 5
Thermal expansion (↑)		
decrease in α	763 ± 10	778 ± 10
region of temperature-	849 ± 5	841 ± 5
dependent α	880 ± 5	869 ± 5
Thermal expansion (↓)		
region of temperature-	776 ± 5	803 ± 10
dependent α	743 ± 10	

direction changes appear with a large hysteresis. For the sample containing 15 mol% Er_2O_3 these effects cannot be ascribed to phase segregation (compare Table 3) because this process is too slow in order to take place during the conductivity measurements. This temperature behaviour was also investigated with high-temperature Guinier (HT Guinier), thermal expansion and differential thermal analysis (DTA). A survey of the results is given in Table 5.

During heating with HT Guinier a broadening of various reflections was observed, however, the (hhh) reflections are not broadened. At about 840 K these broadened reflections transform to distinct lines which are typical for a tetragonal distortion (β^*). This indicates that the broadened reflections are due to a tetragonal distortion which is too small (less than 0.2%) to be measured with HT Guinier. This distortion becomes larger with increasing temperature.

At about 880 K the β^*-phase transforms into an fcc-phase (δ^*), which has a larger lattice constant than the δ-phase.

In the cooling direction no X-ray recording was performed due to Pt-contamination from the gauze at high temperatures of about 900 K. After heating to 950 K we determined about 2% Pt in our specimen (X-ray fluorescence) and this Pt-contamination may greatly influence phase transitions [4].

The thermal expansion of the specimen containing 15 mol% Er_2O_3 is shown in Fig. 6. The shapes of the curves are identical to those of the specimen containing 17.5 mol% Er_2O_3, but the measured effects are smaller.

In the heating direction a decrease in the expansion coefficient α (see arrow) was observed for both samples. In the temperature region of about 845–875 K the apparent value of α is strongly temperature dependent, while at higher temperatures the value of α is again constant (Fig. 6, Table 5), and has about the same value as in the low temperature region. In the cooling direction the changes in the α–T curve appear with a large hysteresis.

DTA revealed no heat effects, which means that they are either very small or are smeared out.

Comparing the data on structural effects with that on conductivity measurements we notice that the temperature region of 730–878 K in which there is a change in E_a agrees well with the region of 750–880 K measured by HT Guinier and the region of 763–875 K measured by thermal expansion. Arguments are the overlap of different temperature intervals with coinciding high-temperature boundaries and the continuous

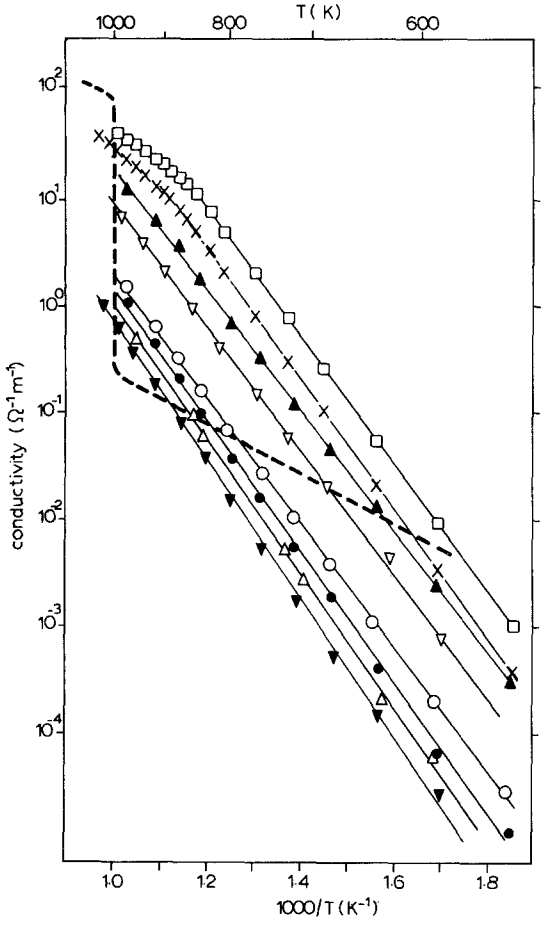

Fig. 5. Conductivity of $(Bi_2O_3)_{1-x}(Er_2O_3)_x$ in air. □, $x = 0.20$; ×, $x = 0.25$; ▲, $x = 0.30$; ▽, $x = 0.35$; ○, $x = 0.40$; ●, $x = 0.455$; △, $x = 0.50$; ▼, $x = 0.60$. The broken line represents the conductivity of pure Bi_2O_3.

(smooth) character at the low-temperature side. The electrical measurements suggest that the tetragonal distortion already starts at 730 K, which could not be measured with HT Guinier and thermal expansion. At 840 K the value of the tetragonal distortion is large enough to be

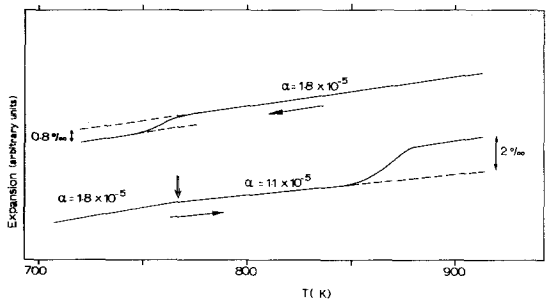

Fig. 6. Heating-up and cooling-down curves as measured with a dilatometer for $(Bi_2O_3)_{0.85}(Er_2O_3)_{0.15}$.

measured and increase strongly with temperature, which agrees with the thermal expansion data (see Table 5).

The sudden increase in the conductivity at 878 K is caused by the structural change from a tetragonal to a cubic phase and at this temperature the value of the expansion coefficient α becomes temperature independent.

The strong decrease in α in the cooling direction can be correlated with the region having a temperature dependent α measured by thermal expansion.

3.3.2. Conductivity of samples containing 20 mol% or more Er_2O_3. The sintered oxides containing 20 mol% or more Er_2O_3 show no jump in the conductivity in the whole range of temperatures examined. However the samples containing 20 mol% and 25 mol% Er_2O_3 showed at about 870 K a knee in the Arrhenius plot, this corresponds to a change in the activation energy and the pre-exponential term, as can be seen from Fig. 5 and Table 4. Takahashi *et al.* found such a knee at about the same temperature for the samples containing 25–33 mol% Y_2O_3 [13], 35–40 mol% Gd_2O_3 [16], and 15 mol% Nb_2O_5 [19]. Bauerle *et al.* [26] and Casselton [27] reported a knee in the Arrhenius plot of yttria stabilized zirconia at about 1070 K; they ascribe this knee to a changing conductivity mechanism. The activation energy changed from 112.8 kJ mol^{-1} to 65.8 kJ mol^{-1} [26]. The absolute values as well as the change in activation energy corresponds with our values and the values measured by Takahashi [13].

Our HT Guinier experiments on Bi_2O_3 based systems revealed that at this temperature the fcc-phase δ, transforms to an fcc-phase with a larger lattice constant. The increase of the lattice constant for $(Bi_2O_3)_{0.80}$ $(Er_2O_3)_{0.20}$ is in the order of 1.5‰. We observed the same phenomena for $(Bi_2O_3)_{0.75}(Er_2O_3)_{0.25}$ and $(Bi_2O_3)_{0.75}$ $(Y_2O_3)_{0.25}$, however the increase in lattice constant was too small to be measured accurately. Therefore we can conclude that the change in activation energy is correlated to a change of the lattice constant.

An increase in the lattice constant of the rhombohedral phase in the system $(Bi_2O_3)_{1-x}$ $(SrO)_x$ with $x = 0.18$–0.43 is reported by

Guillermo *et al.* [28] at about 950–985 K and in the system $(Bi_2O_3)_{1-x}$ $(CaO)_x$ with x = 0.22–0.31 by Conflant *et al.* [29] at about 1000–1010 K. Takahashi *et al.* [6] measured a sudden increase in the conductivity for samples containing 20–40 mol% SrO at about the same temperature as the increase in the lattice constant.

An increase in the unit-cell volume of the cubic fcc phase with constant oxygen ion concentration suggests the possibility of a decrease in the contributions of the local strain component during the passage of oxygen ions through the lattice which leads to a decrease in the activation energy. Before firm conclusions on these aspects can be drawn more has to be known about changes in the ordering of oxygen in the lattice. Details of this subject are under investigation.

In Fig. 7 the oxygen ion conductivity in the Bi_2O_3–Er_2O_3 system is plotted against the Er_2O_3 content at different temperatures. The conductivity of $(Bi_2O_3)_{0.75}$ $(Y_2O_3)_{0.25}$ [13] is given as a reference.

At 573 K and 973 K the logarithm of the conductivity decreases almost linearly with the Er_2O_3 content, whereas between 673 K and 873 K a maximum appears in the conductivity at 20 mol% Er_2O_3. Such a maximum in the fcc-phase region has never before been reported in the literature for investigations on the Bi_2O_3 system [6, 12–19].

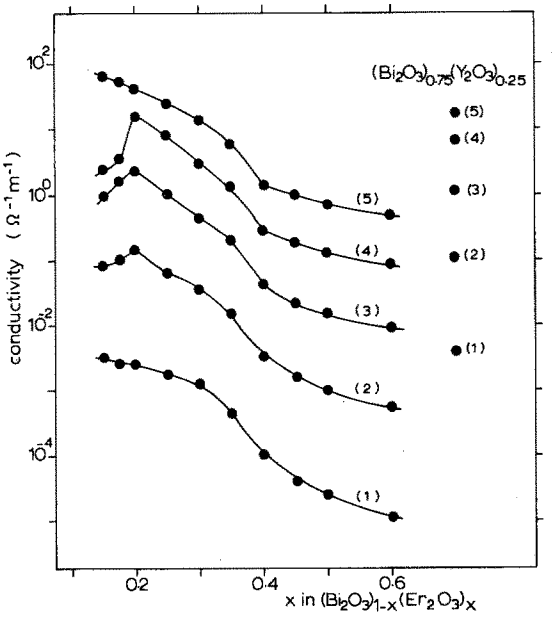

Fig. 7. Conductivity versus composition at different temperatures. The conductivity of $(Bi_2O_3)_{0.75}$ $(Y_2O_3)_{0.25}$ is given as a reference. (1) 573 K; (2) 673 K; (3) 773 K; (4) 873 K; (5) 973 K.

To understand this maximum it is necessary to know more about the discontinuities in the conductivity of the samples containing 15–25 mol% Er_2O_3. Possibly the nature of this maximum can be related to the maximum in the conductivity in the ZrO_2–Y_2O_3 system at concentrations of about 7 mol% as reported,by several authors [30].

Finally it should be mentioned that $(Bi_2O_3)_{0.80}$ $(Er_2O_3)_{0.20}$ is the best oxygen ion conductor yet found. The conductivity at 773 K and 973 K is 2.3 $\Omega^{-1}m^{-1}$ and 37 $\Omega^{-1}m^{-1}$ respectively. The best conductors found by Takahshi were $(Bi_2O_3)_{0.75}(Y_2O_3)_{0.25}$ and $(Bi_2O_3)_{0.85}(Nb_2O_3)_{0.15}$, the conductivity at 773 K is 1.2 $\Omega^{-1}m^{-1}$ and 1.1 $\Omega^{-1}m^{-1}$ respectively and at 973 K 16 $\Omega^{-1}m^{-1}$ and 19 $\Omega^{-1}m^{-1}$ [13, 19]. The conductivity of $(Bi_2O_3)_{0.80}$ $(Er_2O_3)_{0.20}$ is about 50–100 times higher than the conductivity of $(ZrO_2)_{0.915}$ $(Y_2O_3)_{0.085}$ at the same temperatures.

3.4. *Ionic transport number measurements*

In order to determine the charge carriers in these conductors, measurements were performed with an oxygen gas concentration cell. Table 6 shows the ratio of the measured e.m.f. to the theoretical e.m.f. of cell 1. These results indicate that the electrical conduction in the specimens can be almost wholly attributed to the oxygen ion. For the specimens containing 40 mol% or more Er_2O_3 there is an electronic component at low temperatures.

4. Conclusions

High oxygen ion conduction is found in sintered oxides of the Bi_2O_3–Er_2O_3 system. The ionic transference number was found to be equal to one for samples containing 17.5–30 mol% Er_2O_3. Samples containing 40–60 mol% Er_2O_3 showed an electronic component at low temperatures.

The highly conductive fcc phase was stable at low temperatures for substituent concentrations between 17.5–45.5 mol% Er_2O_3. The lower boundary of this region is the smallest percentage valence (III) substituent known in literature which can stabilize the fcc structure at low temperatures.

Between 673–873 K a maximum in the conduc-

Table 6. Ratios of the measured e.m.f. E *to the theoretical value* E_0 *of the following cell:* O_2 *(0.21 atm), Pt* | $(Bi_2O_3)_{1-x}(Er_2O_3)_x$ | *Pt,* O_2 *(1 atm) at different temperatures*

	E/E_0						
x	*773 K*	*823 K*	*873 K*	*923 K*	*973 K*	*1023 K*	*1073 K*
0.175	–	0.98	0.99	1.00	1.01	1.02	1.00
0.20	0.98	1.02	0.98	0.99	0.99	0.99	0.97
0.30	–	0.99	1.02	1.03	1.04	1.03	1.02
0.40	–	–	0.93	0.96	1.00	1.01	1.01
0.50	0.87	0.92	0.95	0.96	0.97	0.97	0.97
0.60	–	0.95	0.95	0.96	0.98	0.98	0.98

tivity was found at 20 mol% Er_2O_3. The most desirable composition in this system is $(Bi_2O_3)_{0.80}(Er_2O_3)_{0.20}$, since the fcc phase is stable at low temperatures and has the highest conductivity over a wide range of temperatures. The conductivity of this specimen is about 2 to 3 times higher than the conductivity of the best oxygen ion conductors reported for Bi_2O_3-based solid solutions and is about 50–100 times higher than the conductivity of stabilized zirconia $(ZrO_2)_{0.915}(Y_2O_3)_{0.085}$ at the same temperature.

We can conclude that sintered oxides of the Bi_2O_3–Er_2O_3 system are promising materials for oxygen gauges and pumps.

Appendix

Small amounts of aluminium were analysed in the following way.

A 100 mg specimen was dissolved in 25 cm^3 hydrochloric acid (1 : 10) and transferred into a 50 cm^3 volumetric flask. 25 cm^3 of the diluted solution was added to a column (the cation-exchange column is pre-treated with 100 cm^3 6 M hydrochloric acid and afterwards with 60 cm^3 0.5 M hydrochloric acid) and the bismuth eluted with 5 x 10 cm^3 0.5 M hydrochloric acid. Subsequently the resin bed was washed,with 125 cm^3 of 3 M hydrochloric acid in 50% ethanol and this eluant was collected in a 500 cm^3 volumetric flask. The aluminium in this solution was then determined [34].

Acknowledgements

The authors are much indebted to Mr. H. Kruidhof for developing a new method for analysing small amounts of aluminium and for performing the chemical analyses. We would like to express our appreciation to Mr J. Boeysma for performing the HT Guinier experiments. Financial assistance from Philips N.V. (Elcoma) is gratefully acknowledged.

References

[1] G. Gattow and H. Schröder, *Z. Anorg. Allg. Chem.* **318** (1962) 176.
[2] E. M. Levin and R. S. Roth, *J. Res. Nat. Bur. Std.* **68A** (2) (1964) 189.
[3] E. M. Levin and C. R. McDaniel *ibid* **69A** (3) (1965) 237.
[4] H. A. Harwig, thesis, State University, Utrecht (1977).
[5] C. N.R. Rao, G. V. Subba Rao and S. Ramdas, *J. Phys. Chem.* **73** (1969) 672.
[6] T. Takahashi, H. Iwahara and Y. Nagai, *J. Appl. Electrochem.* **2** (1972) 97.
[7] G. Gattow und D. Schütze, *Z. Anorg. Allg. Chem.* **328** (1964) 44.
[8] R. Matsuzaki, H. Masumizu and Y. Saeki, *Bull. Chem. Soc. Japan* **48** *(11) (1975) 3397.*
[9] L. G. Sillén, *Arkiv Kemi* **12A** (18) (1937) 1.
[10] *Idem, Krist* **A103** (1941) 274
[11] G. Malmros, *Acta. Chem. Scand.* **24** (1970) 384.
[12] T. Takahashi and H. Iwahara, *J. Appl. Electrochem.* **3** (1973) 65.
[13] T. Takahashi, H. Iwahara and T. Arao, *Ibid* **5** (1975) 187.
[14] T. Takahashi, T. Esaka and H. Iwahara, *Ibid* **7** (1977) 299.
[15] *Idem, ibid* **7** (1977) 303.
[16] *Idem, ibid* **5** (1975) 197.
[17] *Idem, J. Solid State Chem.* **16** (1976) 317.
[18] *Idem, J. Appl. Electrochem.* **7** (1977) 31.
[19] *Idem, J. Electrochem. Soc.* **124** (1977) 1563.
[20] K. W. Browall, *Electrochem. Soc. Spring Meeting* abstract 467 (1978).
[21] L. Heyne, in 'Measurement of Oxygen' (edited by H. Degn *et al.*) Elsevier, Amsterdam, Oxford, N.Y. (1976).
[22] R. K. Datta and J. P. Meehan, *Z. Anorg. Allg. Chem.* **383** (1971) 328.
[23] S. N. Nasonova, V. V. Serebrennikov and G. A. Narnov, *Russ. J. Inorg. Chem.* **18** (1973) 1244.
[24] H. Kruidhof, *Anal. Chimica Acta* **99** (1978) 193.
[25] T. v. Dijk, K. J. de Vries and A. J. Burggraaf,

submitted to *Phys. St. Sol. (A)*.
[26] J. E. Bauerle and J. Hrizo, *J. Phys. Chem. Solids* **30** (1969) 565.
[27] R. E. W. Casselton, *Phys. St. Sol. (A)* **2** (1970) 571.
[28] R. Guillermo, P. Conflant, J. C. Boivin and D. Thomas, *Rev. Chim. min.* **15** (1978) 153.
[29] P. Conflant, J. C. Boivin, and D. Thomas, *J. Solid State Chem.* **18** (1976) 133.
[30] A. I. Ioffe, D. S. Rutman and S. V. Karpachov, *Electrochim. Acta* **23** (1978) 141.